ChemComm

Accepted Manuscript

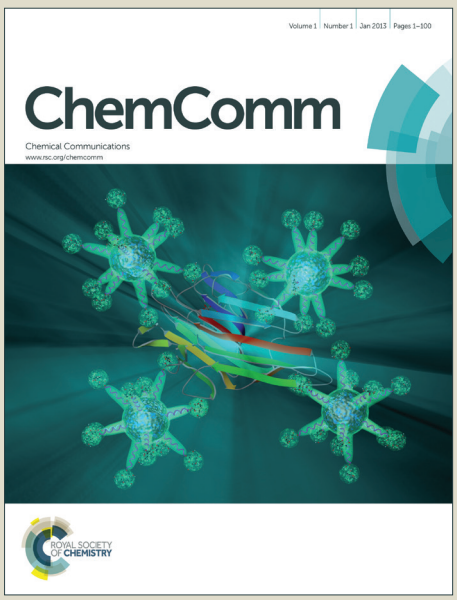

ROYAL SOCIETY OF CHEMISTRY

www.rsc.org/chemcomm

Journal Name

RSCPublishing

COMMUNICATION

Elucidating the Intercalation Mechanism of Zinc Ions into α-MnO_2 for Rechargeable Zinc Batteries

Cite this: DOI: 10.1039/xoxxoooooox

Boeun Lee, Hae Ri Lee, Haesik Kim, Kyung Yoon Chung, Byung Won Cho, Si Hyoung Oh*

Received ooth January 2012,
Accepted ooth January 2012

DOI: 10.1039/xoxxoooooox

www.rsc.org/

The intercalation mechanism of zinc ions into 2 x 2 tunnels of α-MnO_2 cathode for rechargeable zinc batteries was revealed. It involves a series of single and two-phase reaction steps and produces buserite, a layered compound with an interlayer spacing of 11 Å as a discharge product.

Recently, abundant polyvalent cations, such as Mg^{2+}, Zn^{2+}, and Al^{3+}, have been studied as charge transport carriers for new battery systems with high energy densities and the commercial viability necessary for mid to large-scale energy storage systems.[1-4] This trend has gained momentum as the markets for electrical vehicles and load-leveling for intermittent power sources has grown rapidly. For transportation purposes, advanced Li batteries such as Li-air or Li-sulfur cells show promise because of their high energy densities and the capacity for extended driving ranges given a space and weight limit for the vehicles.[5,6] For stationary purposes, energy storage systems with a low material cost and reliable performance are required, where polyvalent ion charge carriers play a pivotal role. Rechargeable zinc batteries are considered one of the best candidates for these applications, as they consist of environmentally friendly materials, such as manganese oxide cathodes, zinc metal anodes, and aqueous electrolyte systems containing $ZnSO_4$ or $ZnCl_2$.[7-10] In addition, this combination is economical to manufacture compared to other polyvalent systems or Li-ion batteries. As for α-MnO_2, its discharge capacity is observed to be approximately 210 mAh g^{-1}, with a practical discharge potential of 1.3 V at a moderate current rate, leading to an energy density of 225 Wh kg^{-1} based on the total weight of electrode materials.[7-10] This is much larger than the values reported for rechargeable magnesium batteries which consist of Mo_6S_8 (Chevrel phase) cathodes and magnesium metal anodes (146 Wh kg^{-1})[1,2]. However, rechargeable zinc batteries employing tunneled manganese dioxide cathodes experience a sharp initial capacity fading and suffer from a poor performance at high current densities. In order to improve the electrochemical properties, the cathode reaction mechanisms must be more thoroughly studied. Recently, our group reported that the intercalation of zinc into the 2 x 2 tunnel of α-MnO_2 ([001] direction) involves a reversible transition of MnO_2 polymorphs from a tunneled to a layered structure (δ-MnO_2) driven by the electrochemical reactions at the cathode.[10] The MnO_2 phase at end of discharge is identified as Zn-birnessite which has a layered structure similar to chalcophanite, $ZnMn_3O_7 \cdot 3H_2O$, but the overall structure is slightly distorted, and hence, adapt itself to a monoclinic space group, P-1.[10-13] The interlayer distance of Zn-birnessite is 7 Å, which is similar to the tunnel size of α-MnO_2.[14-18] During this phase transition, it is observed that the manganese from the tunnel wall is actively dissolved into the electrolyte and at the end of discharge, almost 1/3 of the total manganese in α-MnO_2 is extracted from the structure without collapsing and the electrolyte becomes highly concentrated with manganese ions. However, during the charging process, the ions return to the cathode to reversibly incorporate into the layered structure to construct MnO_6 bridges between the layers thereby forming 2 x 2 tunnels of α-MnO_2.[10] In this work, we show that the intercalation of zinc ions into α-MnO_2 actually leads to the formation of buserite, a layered structure with a much larger interlayer distance (~ 11 Å), after a series of reaction steps and the large stress accompanied by this phase transition causes the gradual collapse of the tunnels or layers upon electrochemical cycling.

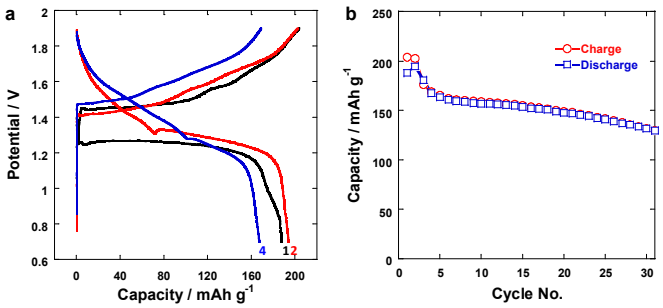

Figure 1. Potential profiles of the zinc/α-MnO_2 Zn-ion battery during the first (black), the second (red), and the fourth (blue) cycles, and (b) their cycling performance up to 30 cycles. The C-rate for the first two cycles was C/20, and thereafter, C/5.

The discharge-charge profiles of the α-MnO_2/zinc battery at the 1st, 2nd and 4th cycles at a current rate of C/20 (1st and 2nd) and C/5 (4th) are shown in **Figure 1a**, where discharge capacities of approximately 195 mAh/g at C/20 and 167 mAh/g at C/5 were observed(1C = 210 mA/g). The α-MnO_2 nanorod was used to

promote fast diffusion of zinc ions into the tunnel as well as to detect any morphological changes. **Figure 1b** indicates that the discharge capacity decreases gradually with cycling and the capacity retention at 30th cycle reached 70%. Plateau potentials at around 1.25 V were observed for the first discharge, indicating that two phases are involved in the electrochemical reaction at this region. However, both plateau and sloping potentials were observed from the 1st charge process. To further investigate the phase evolutions occurring during the electrochemical process, in-situ X-ray diffraction (XRD) patterns were recorded for the initial two successive cycles (**Figure 2**, **Figure S1**). The patterns clearly indicate that a new phase arises because of the interaction of zinc with α-MnO_2 in regions II and III (**Figure 2b, Figure S1**). However, a single phase region is also observed near the very beginning of discharge (region I) and the end of charge (region IV), where characteristic sloping potential is shown in the electrochemical curves. There is a strong peak at 2θ = 8.06^o with less intense peaks at 2θ = 16.18^o and 24.39^o clearly indicating the formation of a layered structure with an interplanar spacing around 11 Å, i.e., buserite.[14,19-22] These peaks can be indexed to reflections from the (001), (002), (003) crystallographic planes, respectively. These peak positions for buserite do not change throughout the whole process, but the intensity grows as the discharge proceeds, indicating that buserite is the product of the reaction of Zn^{2+} ions with α-MnO_2. Buserite is crystallized in an orthorhombic crystal system, one of the most commonly found philomanganates in Mn ocean nodules with a channel width of approximately 10-11 Å , and an important precursor for other types of manganese dioxides.[14] Unlike birnessite, it is suggested that buserite contains extra water layers along the center of the channels.[19-22]

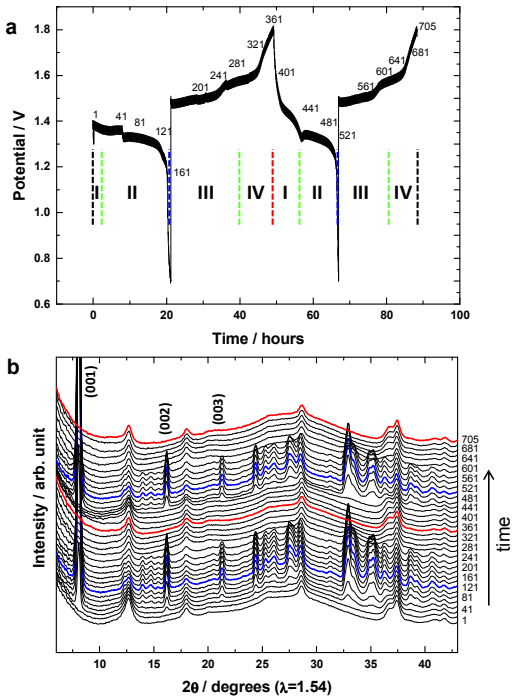

Figure 2. (a) The charge-discharge profile of the zinc/α-MnO_2 for the first two cycles at a scan rate of C/20 (1C = 210 mA/g of the active mass) and (b) the corresponding in-situ XRD patterns during the electrochemical cycling. The regions of interest are described as I, II, III, and IV in (a).

Figure 3a shows several selected XRD patterns from **Figure 2b**. It shows that mixed phases of α-MnO_2 and buserite were observed in the middle of the intercalation/de-intercalation process and the discharge product at 0.7 V mostly consists of buserite, with a minor portion of unreacted α-MnO_2. Furthermore, α-MnO_2 is completely recovered after a full charge up to 1.9 V. Similar patterns are observed for the second cycle shown in **Figure 2b** indicating the process is very reversible. It is reported that this process involves the electrochemical reduction of manganese ($Mn^{4+} + e^- \rightarrow Mn^{3+}$) and the subsequent dissolution of manganese into electrolyte by a chemical disproportionation ($2Mn^{3+} \rightarrow Mn^{4+} + Mn^{2+}(aq)$) during discharge and the intercalation of manganese ions into the buserite channels during the charging process, while zinc ions incorporate into the tunnels during discharge and leave the structure during charging.[10] Therefore, counter-diffusion between Mn^{2+} and Zn^{2+} ions occurs during the electrochemical process in regions II and III. At the beginning of discharge, only zinc ions diffuse into/out of the 2 x 2 tunnel of α-MnO_2, where only a single phase reaction occurs. It is noteworthy that the single phase region for the 2nd discharge is larger than that of the initial discharge. This is most likely due to the presence of potassium ions, which reside in the tunnel that are originally de-intercalated from the structure at the end of the 1st charge. It is reported that these cations at the center of the tunnel in α-MnO_2 are extractable without the tunnel collapsing.[17] Without these K^+ ions, Zn^{2+} ions can infiltrate more freely into the tunnel during the discharge process.

In aqueous solutions, Zn^{2+} ions are typically octahedrally coordinated with water molecules, such as $[Zn(H_2O)_6]^{2+}$.[4] However, the water molecules in this complex are strongly polarized by the high charge density of the central divalent cation. This leads to the spontaneous hydrolysis reaction (1):

$$[Zn(H_2O)_6]^{2+} + H_2O \leftrightarrows [Zn(H_2O)_{6-h}(OH)_h]^{(2-h)+} + h\ H_3O^+ \quad (1)$$

where the equilibrium constant (K) and the degree of hydrolysis (h) depend on the pH of the solution. At a pH 4(pH of the electrolyte solution), h is estimated to be close to 1.9. This implies that at pH 4, one or more than one OH^- group is coordinated to zinc ion and the effective charge from the complex would be diminished, since the high ionic charge of the central cation is screened by the coordinating OH^- group and distributed by the partial charges formed by polarized intimate water molecules. This is very important in terms of the diffusion of Zn^{2+} ions through the tunnels and channels, as the electrostatic interactions arise between Zn^{2+} ions and the framework of the MnO_2 hosting material. Since the width of the buserite tunnel is large (approximately 11 Å), zinc ions may move through the channel with water molecules still coordinated as a form of $[Zn(H_2O)_{6-h}(OH)_h]^{(2-h)+}$ so that the charge of the Zn^{2+} ion is partly shielded. In layered MnO_2 compounds, Zn^{2+} ions are known to adopt octahedral configurations on the manganese vacancy site coordinated with three oxygen atoms adjacent to vacancy sites and three from water molecules inside the channel when the amount of Zn^{2+} ions is large.[23-25] When the amount of Zn^{2+} ions less, the ions adopt a tetrahedral coordination above/below the manganese vacancy site with one water molecule.[23-25] Including these coordinated water molecules, buserite is known to have triple water layers in the channels, which may aid in the insertion or removal of zinc ions.

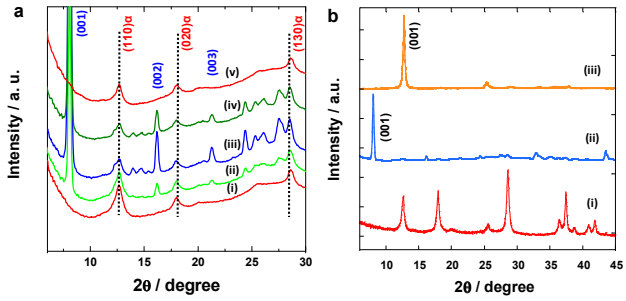

Figure 3. (a) Selected in-situ XRD patterns from Figure 2b; (i) un-discharged-(1), (ii) partially-discharged-(41), (iii) fully-discharged-(141), (iv) partially-charged-(261), and (v) fully-charged-(281) electrodes. The number in brackets represents the XRD pattern number. (b) (i) XRD patterns for α-MnO_2, (ii) in-situ XRD pattern for the discharged electrode, and (iii) ex-situ XRD pattern for the discharged electrode after drying in the oven.

The chemical diffusion coefficient (D_M) of polyvalent cations through the tunnel or channel of the cathode materials for single and two-phase regions was determined by the galvanostatic intermittent titration technique (GITT)[26,27] and is shown in **Figure 4**. It is also observed that the diffusion coefficient for the single phase region (region I, IV) is larger than that for the two-phase region primarily because reactions in the two-phase region occur only at the interface of two phases, while reactions in the single phase occur in many places in the nanorod.[28-31] But these values are much smaller than that for Li^+ ions reported in the literature[32], since the activation barrier for the diffusion of divalent Zn^{2+} is considered much larger due to the higher Coulombic interactions. **Figure 3b** shows the XRD patterns of discharged electrode material dried in an oven that indicate the shift of the (001) reflection of buserite to a much higher angle with an interlayer distance of 7 Å. This corresponds to the phase transition from buserite to birnessite upon removal of water molecules from the layer.[21] It is well-known that buserite is not stable when the extra-water layers are removed from the channel after drying; it shrinks to a more stable layered structure having narrower channels. Therefore, the previously observed Zn-birnessite is attributed to water loss from the original buserite structure. These processes are schematically shown in **Figure S2**, where the tunneled-to-layered transition in MnO_2 polymorphs is triggered by the electrochemical insertion of zinc and the shrinkage that occurs in the channel width upon drying.

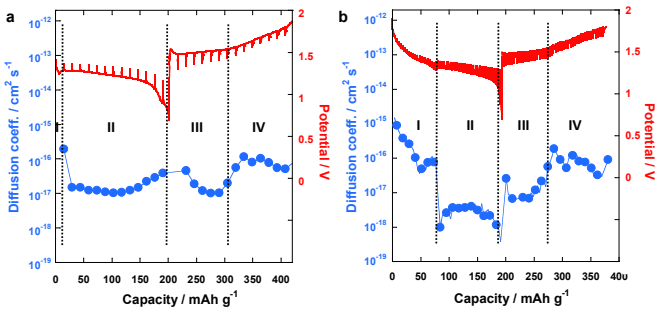

Figure 4. Variation of diffusion coefficient for Zn2+ ions and potential profiles during (a) the first and (b) the second discharge and charge processes measured by GITT. It is noteworthy that the diffusion coefficient for the single phase region (I, IV) is calculated to be higher than those for the two-phase region (II. III).

The high-resolution transmission electron microscopy (HR-TEM) images in **Figure S3** show that the original nanorod morphology of α-MnO_2 and internal tunnel or channel structure is well-preserved after the discharge and re-charge, implying that the structures of the original, discharged, and recharged cathodes are closely related. Specifically, the layered structure of birnessite is clearly observed although it was created by the shrinkage of the buserite. A closer inspection of the TEM images in **Figure S3** shows that in addition to nanorods, scraps of small particles were found on the surface of the nanorods, especially on the dried discharged electrode. Elemental analyses of these scraps and the nanorod in **Figure S4** show that although the overall composition between Zn and Mn for nanorods and scraps together is similar to 3.0 (region C) as observed previously, which is the ratio for chalcophanite ($ZnMn_3O_7 \cdot 3H_2O$), the scraps (region D) were observed to be Zn-rich oxides ($Zn_{1-x}Mn_xO$), whereas the Zn content in the nanorod (region B) is relatively less. This suggests that Zn-birnessite cannot hold as many zinc ions inside its tunnels as Zn-buserite does, because the tunnel size decreases dramatically and the electrostatic interaction between zinc ions increases sharply during the drying process. Therefore, it is reasonable to assume that these zinc-rich oxides were most likely formed during the drying process as zinc ions and water molecules are discharged from the channel.

The large volumetric changes between α-MnO_2 and Zn-buserite can trigger a great deal of residual structural stresses during the electrochemical cycling. This can lead to the collapse of the layered structure upon repeated cycling. Previous research reports that the growth of an amorphous phase occurs as the electrochemical cycling proceeds, with a decrease in the discharge capacity.[10] In terms of structural stability during cycling, it would be advantageous to have a tunnel with a size comparable to the initial buserite layer width. Therefore, a good candidate material would be todorokite which has a 3 x 3 tunnel size (~ 10 Å) with a similar intercalation mechanism.[33] It has been reported that the cyclic stability of todorokite is better than α-MnO_2 although it has a smaller capacity.[9] These findings gives a hint on developing cathode materials for other energy storage systems based on the intercalations of multivalent cations. The detailed reaction mechanism for this material is currently being studied, the results of which will be reported in a later communication.

Conclusions

The correct intercalation mechanism of zinc ions into α-MnO_2 during electrochemical cycling was reported. The mechanism involves a reversible phase transition between tunneled (α-MnO_2) and layered (Zn-buserite) MnO_2 polymorphs, which is induced by a series of single- and two-phase electrochemical reactions on the cathode. It turns out that the previously observed Zn-birnessite is not a direct reaction product of zinc insertion into α-MnO_2, but is formed by the loss of the intercalated zinc ions and water molecules from the layers of buserite.

This work was supported by the Dream Project funded by the Korea Institute of Science and Technology [KIST-2013-2E23996]] and the Secondary Battery R&D program of MOTIE/KEIT, [10042840, Development of LMO cathode material of high capacity(≥120 mAh/g) and high density(≥2.0g/mL) for EV.

Notes and references

Korea Institute of Science and Technology, Hwarang-ro 14-gil 5, Seongbuk-gu, Seoul, 136-791, Korea. Email : sho74@kist.re.kr
* Corresponding author.

† Electronic Supplementary Information (ESI) available: Experimental details, GITT calculation. See DOI: 10.1039/b000000x/

1 D. Aurbach, Z. Lu, A. Schechter, Y. Gofer, H. Gizbar, R. Turgeman, Y. Cohen, M. Moshkovich and E. Levi, *Nature*, 2000, **407**, 724.
2 E, Levi, Y. Gofer and D. Aurbach, *Chem. Mater.*, 2010, **22**, 860
3 N. Jayaprakash, S. K. Das and L. A. Archer, *Chem. Commun.*, 2011, **47**, 12610.
4 W. Wang, B. Jiang, W. Xiong, H. Sun, Z. Lin, L. Hu, J. Tu, H. Zhu and S. Jiao, *Sci. Rep.*, 2013, **3**, 3383.
5 P. G. Bruce, S. A. Freunberger, L. J. Hardwick and J. -M. Tarascon, *Nat. Mater.*, 2012, **11**, 19.
6 X. Ji, K. T. Lee and L. F. Nazar, *Nat. Mater.*, 2009, **8**, 500.
7 C. Xu, B. Li, H. Du and F. Kang, *Angew. Chem. Int. Ed.*, 2012, **51**, 933.
8 C. Xu, B. Li, S. W. Chiang, J. Ma and F. Kang, *J. Electrochem. Soc.*, 2013, **160**, A93.
9 J. Lee, J. B. Ju, W. I. Cho, B. W. Cho and S. H. Oh, *Electrochim. Acta*, 2013, **112**, 138.
10 B. Lee, C. S. Yoon, H. R. Lee, K. Y. Chung, B. W. Cho and S. H. Oh, *Sci. Rep.*, 2014, **4**, 6066.
11 A. D. Wadsley, *Nature*, 1953, **172**, 1103.
12 A. D. Wadsley, *Acta Cryst.*, 1955, **8**, 165.
13 J. E. Post and D. E. Appleman, *Am. Miner.*, 1988, **73**, 1401.
14 J. E. Post, *Proc. Natl. Acad. Sci.*, 1999, **96**, 3447.
15 M. M. Thackeray, *Prog. Solid St. Chem.*, 1997, **25**, 1.
16 B. J. Aronson, A. K. Kinser, S. Passerini, W. H. Smyrl and A. Stein, *Chem. Mater.*, 1999, **11**, 949.
17 M. H. Rossouw, D. C. Liles, M. M. Thackeray, W. I. F. David and S. Hull, *Mat. Res. Hull*., 1992, **27**, 221.
18 Q. Feng, K. Yanagisawa and N. Yamasaki, *J. Porous Mater*., 1998, **5**, 153.
19 A. Manceau, V. A. Drits, E. Silvester, C. Bartoli and B. Lanson, *Am. Mineral.*, 1997, **82**, 1150.
20 J. Luo, Q. Zhang, A. Huang, O. Giraldo and S. L. Suib, *Inorg. Chem.*, 1999, **38**, 6106.
21 D. C. Golden, C. C. Chen and J. B. Dixon, *Clays Clay Miner*., 1987, **35**, 271.
22 M. J. Duncan, F. Leroux, J. M. Corbett and L. F. Nazar, *J. Electrochem. Soc*., 1998, **145**, 3746.
23 M. Villalobos, B. Lanson, A. Manceau, B. Toner and G. Sposito, *Am. Mineral.*, 2006, **91**, 489.
24 K. D. Kwon, K. Refson and G. Sposito, *Geochim. Cosmochim. Acta*, 2009, **73**, 1273.
25 B. Toner, A. Manceau, S. M. Webb and G. Sposito, *Geochim. Cosmochim. Acta*, 2006, **70**, 27.
26 W. Weppner and R. A. Huggins, *Electrochem. Soc.*, 1977, **124**, 1569.
27 C. J. Wen, B. A. Boukamp and R. A. Huggins, *Electrochem. Soc.*, 1979, **126**, 2258.
28 M. Wagemaker, W. J. H. Borghols and F. M. Mulder, *J. Am. Chem. Soc.*, 2007, **129**, 4323.
29 M. Okubo, E. Hosono, J. Kim, M. Enomoto, N. Kojima, T. Kudo, H. Zhou and I. Honma, *J. Am. Chem. Soc.*, 2007, **129**, 7444.
30 A. Yamada, H. Koizumi, S. -I. Nishimura, N. Sonoyama, R. Kanno, M. Yonemura, T. Nakamura and Y. Kobayashi, *Nat. Mater*., 2006, **5**, 357.
31 P. Gibot, M. Casas-Cabanas, L. Laffont, S. Levasseur, P. Carlach, S. Hamelet, J. -M. Tarascon and C. Masquelier, *Nat. Mater.*, 2008, **7**, 741.
32 N. Kumagai, T. Sasaki, S. Ositari and S. Komaba, *J. New Mat. Electrochem. Systems*, 2006, **9**, 175.
33 Q. Feng, *Chem. Mater*., 1995, **7**, 1722.